Journal of The
Electrochemical Society

OPEN ACCESS

A Redox-Electrodialysis Model with Zero Fitting Parameters: Insights into Process Limitations, Design, and Material Interventions

To cite this article: Timothy C. Hudak *et al* 2024 *J. Electrochem. Soc.* **171** 053502

View the article online for updates and enhancements.

You may also like

- Brackish ground water and dairy wastewater treatment using electrodialysis system
Dipak Ankoliya, Anurag Mudgal, Manish Kumar Sinha et al.
- Electrodialysis for Removal of Impurities in Silver Electrowinning
Pauline Zimmermann, Önder Tekinalp, Liyuan Deng et al.
- Investigation Into Rejuvenation of Spent Chromium Plating Solutions by Bipolar Membrane Electrodialysis
Jie Zhao, Guofeng Cui and Hong Liu

PAT-Tester-x-8 Potentiostat:
Modular Solution for Electrochemical Testing!

EL-CELL®
electrochemical test equipment

- Flexible Setup with up to 8 Independent Test Channels!
  Each with a fully equipped Potentiostat, Galvanostat and EIS!
- Perfect Choice for Small-Scale and Special Purpose Testing!
  Suited for all 3-electrode, optical, dilatometry or force test cells from EL-CELL.
- Complete Solution with Extensive Software!
  Plan, conduct and analyze experiments with EL-Software.
- Small Footprint, Easy to Setup and Operate!
  Usable inside a glove box. Full multi-user, multi-device control via LAN.

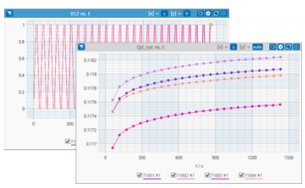

Scan me!

Contact us:
+49 40 79012-734
sales@el-cell.com
www.el-cell.com

This content was downloaded from IP address 130.202.234.13 on 26/03/2025 at 13:02

Journal of The Electrochemical Society, 2024 **171** 053502

A Redox-Electrodialysis Model with Zero Fitting Parameters: Insights into Process Limitations, Design, and Material Interventions

Timothy C. Hudak,[1,*] Christopher A. Gorski,[2,*,z] and Christopher G. Arges[1,a,*,z]

[1]*Department of Chemical Engineering, The Pennsylvania State University, University Park, Pennsylvania 16802, United States of America*
[2]*Department of Civil and Environmental Engineering, The Pennsylvania State University, University Park, Pennsylvania 16802, United States of America*

Redox-Electrodialysis (r-ED) is an electrochemical desalination cell architecture that has recently received considerable interest, due to its low energy demand relative to electrochemical desalination technologies that rely on electrode-based ion removal. To further improve the energy efficiency of r-ED, we developed a lumped mathematical model with no adjustable parameters to investigate the various sources of overpotential within the cell. Existing models of electrodialysis and r-ED cells either do not accurately incorporate all phenomena contributing to the overpotential or utilize empirical fitting parameters. The model developed here indicates that ohmic overpotentials, especially in the diluate chamber, are the most significant contributors to energy losses. Based on this insight, we hypothesized that adding an ion exchange resin wafer in the diluate compartment would increase the ionic conductivity and decrease the energy demand. Experimental results showed an 18% reduction in specific energy use while achieving the same degree of salt removal (20 mM to 12 mM). Furthermore, the resin wafer enabled complete desalination to potable drinking levels at a current density previously unachievable within practical operating voltage limits (4.93 mA cm^{-2}). We also expanded the model to explore differences in r-ED energy use between configurations using multiple cells and a single cell with increased area.

© 2024 The Author(s). Published on behalf of The Electrochemical Society by IOP Publishing Limited. This is an open access article distributed under the terms of the Creative Commons Attribution 4.0 License (CC BY, http://creativecommons.org/licenses/by/4.0/), which permits unrestricted reuse of the work in any medium, provided the original work is properly cited. [DOI: 10.1149/1945-7111/ad3d0e]

Manuscript submitted February 5, 2024; revised manuscript received March 19, 2024. Published May 8, 2024.

Supplementary material for this article is available online

The United Nations estimates that approximately 2 billion people reside in regions without access to well-managed drinking water services.[1] Other estimates indicate approximately 4.3 billion people, over 70% of the global population, face water scarcity for at least one month a year.[2] Considering significant population growth in the coming decades, even nations that currently meet annual water demands will need to drastically increase production.[3] These figures highlight the need for increased access to stable water resources, which can be addressed using more saline water sources that are far more abundant than freshwater (<500 ppm total dissolved solids, TDS). Specifically, seawater (~35,000 ppm TDS) and brackish groundwater (1,000–10,000 ppm TDS) can potentially be treated with desalination technologies to meet global freshwater demands.[4–6]

While Reverse Osmosis (RO) is a mature, cost-effective, and energy-efficient process for seawater desalination, drawbacks include significant capital costs, large units, and high-pressure requirements to drive water across the membrane. These attributes are often unfeasible for small, mobile, or poor auxiliary infrastructure operations. Electrochemical separation methods, such as electrodialysis (ED), do not require high-pressure operation; thus, they enable a simpler downscaling for distributed production. Electrochemical separations generate an electric field perpendicular to fluid flow, subsequently driving ions across alternating cation exchange membranes (CEMs) and anion exchange membranes (AEMs).[7] Furthermore, a theoretical analysis indicates electrochemical processes can enable lower energy consumption at concentrations within the brackish water regime, approximately 4,500 ppm and lower.[8]

Redox-electrodialysis (r-ED), which is similar to ED, utilizes kinetically facile and chemically stable redox-active compounds in lieu of hydrogen evolution and oxygen evolution reactions at the cathode and anode, respectively. The reasons for growing interest in r-ED in recent years are twofold. First, initial experimental comparisons between r-ED and membrane capacitive deionization (MCDI) architectures clearly demonstrate r-ED's superior performance in terms of energy consumption metrics.[9] Considering that r-ED's mechanism is electromigration compared to MCDI's electrosorption, these results reaffirm similar comparisons between MCDI and traditional ED devices.[10] Second, the cost of electrodes can be significantly reduced by using carbon instead of expensive mixed metal oxides (e.g., RuOx and IrOx) while also decreasing energy demands associated with the electrodes (Fig. 1).[9,11–20]

Understanding the relationships among cell design, process operating parameters, production rates, and associated energy demands is critical for identifying cases of practical feasibility and understanding the technological limits of the r-ED platform. For example, comparing cells in series with a single consolidated stack is challenging to explore experimentally due to the complexity of constructing and operating multiple cells. Device modeling is a beneficial tool to provide insight into these questions. While models of ED exist in the literature, they do not account for the unique geometry of an r-ED cell (i.e., three membranes per cell pair); the electrode rinse solutions differing in ionic species and concentrations; and the reduction and oxidation of soluble redox-active compounds at the electrode surfaces as opposed to hydrogen and oxygen evolution.[21,22] Furthermore, electrode kinetics are typically ignored due to the low overpotential contribution to an electrodialysis stack compared to ohmic overpotentials, yet electrode kinetics may play a considerable role in an r-ED voltage (or current) profile. Some attempts have been made to model the r-ED platform, but they employ empirical fitting parameters, such as process time constants and ambiguous overpotential terms, to fit system outputs (i.e., how the salt concentration in the concentrate, the salt concentration in the diluate, and the cell voltage vary over time).[14]

In this work, a series of r-ED experiments were carried out at multiple operating conditions. A robust r-ED model was developed to mimic the experimental setup, capturing relevant overpotentials, energy demands, and production rates. The model includes activation overpotentials for ferrocyanide/ferricyanide charge-transfer

*Electrochemical Society Member.
[a]Present address: Argonne National Laboratory, Lemont, IL, 60439. United States.
[z]E-mail: cag981@psu.edu; cga5126@psu.edu

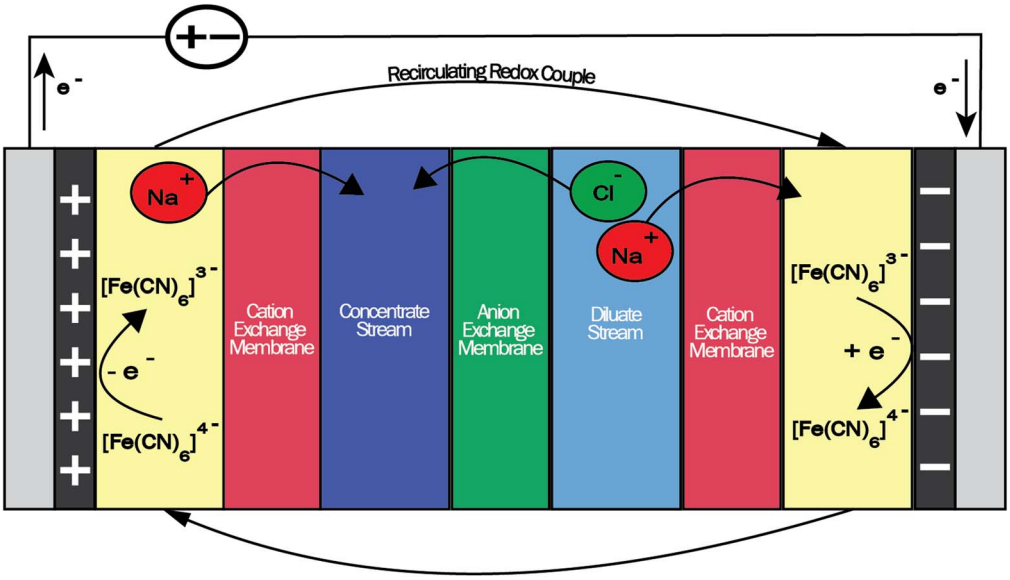

Figure 1. A diagram of a redox-electrodialysis cell using a ferro/ferricyanide redox couple.

kinetics, as well as ohmic overpotentials arising from ion transport in the liquid electrolytes, CEMs, AEMS, and associated boundary layers. It also accounts for junction overpotentials, which occur due to ion activity differences between compartments. Moreover, no adjustable fitting parameters are used; instead, all parameters are design specific or estimated based on external experiments and existing literature. A quasi-Monte Carlo approach was used to capture intrinsic system variabilities. Sobol sensitivity analysis was employed to elucidate which parameters have a large effect within the system. Ultimately, the model indicates that ohmic losses in the diluate stream represent the largest source of overpotential when compared to other overpotential terms. The large resistance in the diluate stream arises from ion depletion. Furthermore, employing the model in theoretical case studies altering the facility of electrode reactions indicates that only marginal gains in energy reduction can be expected with kinetically superior redox compounds.

Ion-exchange resin wafers (RWs) are a known class of porous ionic conductors that are used to reduce the ohmic losses in low conductivity process streams (e.g., electrodeionization units). RWs employ ion exchange resin particles that are held together by a polymer binder (e.g., polyethylene, latex, or ionomers). By serving as a conductive pathway for ions in solution, porous ionic conductors can increase the ionic conductivity of a diluate channel throughout the entire duration of the desalination, subsequently reducing energy requirements.[23–28] To illustrate how effective the RW is for curtailing ohmic losses and reducing energy expenditure, we deployed an unoptimized mixed cation and anion exchange RW in the diluate chamber to ameliorate ohmic resistance, lowering the overall energy demand for desalination. Finally, the model demonstrates that a r-ED configuration with multiple cells in series are more energy efficient when compared to scaled-up cell, consolidated device.

Methods

Cell construction.—A custom-built, four-channel flow cell was manufactured and used for all r-ED desalination experiments. Channels were separated by one Fumasep FAS-PET-75 anion exchange membrane (AEM) and two Fumasep FKD-PK-75 cation exchange membranes (CEMs) (purchased from Fuel Cell Store). The cell was assembled in dry form and rinsed with NaCl solution upon construction to test for leaks and to equilibrate the membranes. The geometric area of the cell is 7.00 cm × 3.65 cm, where each channel has a woven nylon mesh space with an open area fraction of 0.44. Using a micrometer, the measured thickness was approximately 1 mm. Approximately 7 cm × 3 cm carbon-felt electrodes were immersed in 1 M nitric acid solution at 95 °C for three hours. After acid treatment, electrodes were rinsed several times with DI water and dried. The dry carbon felts were then adhered to graphite paper using a 1 ml aliquot of a slurry composed of 1.4 wt% PVDF, 4.4 wt % carbon black, and 94 wt% NMP and dried overnight under vacuum.

Desalination experiments.—All desalination experiments utilized electrode rinse solutions of 40 mM $K_3Fe(CN)_6$, 40 mM $Na_4Fe(CN)_6$, and 50 mM Na_2SO_4 (Millipore Sigma); DI water used for solutions had a resistivity of 18.2 MΩ·cm. All experiments were operated in batch mode, with recirculating diluting and brine solutions. For experiments operating at 50% water recovery, reservoir volumes of 40 ml were used. For experimental operating at ≈71% water recovery, reservoir volumes of 20 ml (brine) and 50 ml (diluate) were used. Two initial feed concentrations within the brackish water regime, 50 mM and 20 mM, were chosen to produce greater variation to the operating conditions for model validation. All process stream reservoirs were continuously mixed using a stir bar. Flow rates of all compartments were 36 ml min^{-1} across all batch experiments and is specified for single-pass experiments. In-line conductivity probes (Microelectrodes Inc.) were placed in the tubing near the concentrate and diluate compartment inlets to measure reservoir concentrations for batch experiments. For single-pass experiments, probes were moved to their respective outlets. Note that compartments were rinsed with the appropriate feed solution between each desalination run.

Resin wafer (RW) fabrication and conductivity measurements.—A mixed ion exchange RW used a ratio of 1:1.3 cation exchange to anion exchange resins.[23] Resin particles were added to low-density polyethylene binder and sodium chloride porogen in the ratio of 2.0:1.0:0.5 and packed into a mold. The mold was then hot-pressed at a force of two metric tonnes at approximately 100 °C for 30 min and was allowed to cool overnight under force. To remove the porogen, the RW was repeatedly submerged in fresh DI water for ∼30 min, at least three times.[23] The RW was soaked in 20 mM NaCl solution for approximately 30 min to allow for swelling before cell construction. The swollen wafer thickness was 1.41 ± 0.01 mm. RW conductivity measurements were taken ex situ by placing a 5 cm × 2.5 cm slide between two platinum foils of the same size. The entire

assembly, including the leads, was then submerged in NaCl solutions of varying ionic strength to allow for equilibration. Potentiostatic electrochemical impedance spectroscopy (EIS) was then used to measure high-frequency resistance. The high-frequency resistance was determined when the phase angle was equal to zero.

Area-specific resistance measurements.—Potentiostatic EIS was employed in a full-cell, two-electrode setup. The applied AC voltage was 10 mV root mean squared, ranging from at least 100 kHz to 1 Hz. The high-frequency resistance was then determined where the phase angle was approximately equal to zero.

Junction potential measurements.—An H-cell setup was utilized for both AEM and CEM junction potential measurements. Stirring was present in both compartments with Ag/AgCl reference electrodes situated in Luggin capillaries placed as close as physically possible to the surface of the membrane separating the two compartments. A range of NaCl solution concentrations, similar to what would be observed in a desalination experiment, were used for AEM junction potential measurements. For CEM junction potential measurements, the concentration of the solution modeling the outer compartments was held constant. In contrast, the NaCl concentration was varied over the concentration range expected during a desalination experiment. The potential difference observed was recorded for 200 s and averaged over the duration for both AEM and CEM measurements.

Modeling - mass balances.—For a batch separation process, we begin with mass balance expressions for the concentrate, diluate, and electrode rinse recirculating reservoirs, assuming that the time delays for the solutions to be pumped from the reservoir to the cell and back are negligible.

$$V_C^T \frac{dC_C^T}{dt} = Q_C(C_C^C - C_C^T) \quad [1]$$

$$V_D^T \frac{dC_D^T}{dt} = Q_D(C_D^C - C_D^T) \quad [2]$$

$$V_R^T \frac{dC_R^T}{dt} = Q_R(C_R^C - C_R^T) \quad [3]$$

where subscripts C, D, and R correspond to the concentrate, diluate, and electrode rinse streams and superscripts C and T indicate the cell's compartment or external tank reservoir, respectively. V is the volume, C corresponds to the time-dependent concentration of NaCl in a particular stream, and Q is the volumetric flowrate of the stream.

For redox-ED cell chambers, we follow an approach similar to Ortiz et al. and Wright et al., where the general mass balances for the concentrate and diluate cell chambers account for bulk flow, migration and assume steady-state diffusion across the IEMs.[21,22] Furthermore, the electrode rinse is treated as an ion source only due to diffusion (i.e., the net change in ion concentration due to migration is zero).

$$V_C^C \frac{dC_C^C}{dt} = Q_C(C_C^T - C_C^C) + \frac{\phi I}{zF} - \frac{AD_a(C_C^{wa} - C_D^{wa})}{l_a} + \frac{AD_c(C_R^{wcc} - C_C^{wc})}{l_c} \quad [4]$$

$$V_D^C \frac{dC_D^C}{dt} = Q_D(C_D^T - C_D^C) - \frac{\phi I}{zF} + \frac{AD_a(C_C^{wa} - C_D^{wa})}{l_a} + \frac{AD_c(C_R^{wcd} - C_D^{wc})}{l_c} \quad [5]$$

$$V_R^C \frac{dC_R^C}{dt} = Q_R(C_R^T - C_R^C) - \frac{AD_c(C_R^{wcd} - C_D^{wc})}{l_c} - \frac{AD_c(C_R^{wcc} - C_C^{wc})}{l_c} \quad [6]$$

where ϕ is the current efficiency, I is the applied current, z is the ion valence, F is Faraday's constant, A is the active membrane area, and D_a and D_c are the diffusion coefficients of NaCl in the anion and cation exchange membranes respectively and are assumed to be equal. Here, l_a is the thickness of the AEM, and l_c is the thickness of the CEM. Superscripts *wa* and *wc* indicate the surface concentrations of the AEM and CEM diluting and concentrating compartments, respectively. In contrast, superscripts *wcc* and *wcd* indicate the surface concentrations in the electrode rinse compartment at the concentrating and diluting CEM. We assumed a current efficiency of 1 for this model because the cell was sealed (i.e., no shunt currents that arise from saline leakage), and the voltage was limited to 1.6 V (to mitigate parasitic reactions like water electrolysis and electrode corrosion). Water transport across the ion exchange membranes is a known phenomenon in electrochemical systems.[21,29–32] However, we assumed that the reservoir and compartment volumes were constant throughout the desalination experiment. Although this assumption is common in the literature, experimental evidence from this study suggests that the reservoir masses can change by 2%–5% during desalination due to osmosis and electro-osmosis, which is negligible for this study's analysis. Also note that Eqs. 4–6 assume that the compartments are well-mixed with no concentration gradients. Although concentration gradients may exist, particularly in cases of low residence times, this work does not attempt to account for such gradients.

To solve for the concentrations at the surface of the membranes, the total ion flux is equated to the summation of fluxes due to migration and diffusion. Considering the four-channel geometry of the cell, we arrive at the following two expressions for the AEM;

$$\frac{\phi I}{zF} = \frac{t^- \phi I}{zF} + k_m(C_D^C - C_D^{wa})A \quad [7]$$

$$\frac{\phi I}{zF} = \frac{t^- \phi I}{zF} + k_m(C_C^{wa} - C_C^C)A \quad [8]$$

where t^- indicates the transference number of the anion, k_m is the overall mass transfer coefficient, and A is the membrane area. Similarly, for the CEMs, we arrive at the following four expressions:

$$\frac{\phi I}{zF} = \frac{t^+ \phi I}{zF} + k_m(C_D^C - C_D^{wc})A \quad [9]$$

$$\frac{\phi I}{zF} = \frac{t^+ \phi I}{zF} + k_m(C_C^{wc} - C_{Con}^C)A \quad [10]$$

$$\frac{\phi I}{zF} = \frac{t^+ \phi I}{zF} + k_m(C_R^{wcd} - C_R^C)A \quad [11]$$

$$\frac{\phi I}{zF} = \frac{t^+ \phi I}{zF} + k_m(C_R^C - C_R^{wcc})A \quad [12]$$

where t^+ indicates the transference number of the cation. While the transference number of a particular ion can vary with concentration, reported t^+ values for NaCl vary from 0.3918 to 0.3821 over the concentration range of 0.01 M to 0.2 M.[33] Therefore, transference numbers were assumed to be constant values of $t^+ \approx 0.39$ and $t^- \approx 0.61$. To extend the analysis to other salt species or

multicomponent salt mixtures, Eq. S1 can be employed to estimate ion transference numbers in the absence of measured values.

It is important to note that we avoided negative surface concentration values at very dilute regimes when solving the model. In other words, if the surface concentration is calculated to be less than zero, the surface concentration is set to a value of 0 mM.

Modeling - estimation of the mass transfer coefficient.—To calculate the overall mass transfer coefficient, we adopt a geometric treatment of woven rhomboidal spacers originally developed by Costa et al. and used previously throughout the literature.[21,34–36] For a rhomboidal mesh where filaments are of equal diameter, and the filament weave is perpendicular, the void fraction, ϵ was calculated by:

$$\epsilon = 1 - \frac{\pi d_f^2}{2 l_m h} \quad [13]$$

where d_f is the filament diameter, l_m is the distance between filaments, and h is the thickness of the mesh. The hydraulic diameter, d_h, of the channel is calculated by an equation developed by Schock and Miquel:[37]

$$d_h = \frac{4\epsilon}{\left(\frac{2}{h}\right) + (1-\epsilon)\frac{4}{d_f}} \quad [14]$$

Reynolds (Re) and Schmidt (Sc) numbers are calculated by

$$Re = \frac{u d_h}{\nu} \quad [15]$$

$$Sc = \frac{\nu}{D} \quad [16]$$

where u is the fluid velocity in the channel, ν is the kinematic viscosity of the solution, and D is the diffusion coefficient of NaCl in water at infinite dilution. It is assumed that the kinematic viscosity is that of pure water given the relatively low concentrations of NaCl. The Sherwood number (Sh) is defined as ratio of convective to diffusive mass transfer rates and is proportional to the Reynolds and Schmidt numbers. The mass transfer correlation was used below to estimate the overall mass transfer coefficient, k_m:[34]

$$Sh = \frac{k_m d_h}{D} = 0.664 k_{corr} Re^{0.5} Sc^{0.33} \left(\frac{2 d_h}{l_m}\right)^{0.5} \quad [17]$$

where k_{corr} is a correction factor estimated from the spacer geometry.

$$k_{corr} = 1.654 \left(\frac{d_f}{h}\right)^{-0.039} \epsilon^{0.75} \left(\sin\frac{\theta}{2}\right)^{0.086} \quad [18]$$

The angle, θ, is the hydrodynamic angle, in this case the angle between two spacer filaments, and $\theta \approx 90°$ in this work.

Modeling—cell thermodynamics.—The following overall expression for a junction, defined as the difference in electric potential between phases β and α, has been derived in the literature and will not be done here.[33,38]

$$E_J = -\frac{RT}{F} \sum_j \int_\alpha^\beta \frac{t_j}{z_j} d \ln a_j \quad [19]$$

where index $j = +$ or $-$, t_j indicates the membrane permselectivity for the CEM or AEM, respectively, and ranges from 0 to unity, where unity is a perfectly selective membrane, and z_j is the valence of the ionic species. The activity of an ion species is represented by a_j. The activity can further be represented as the product of the mean activity coefficient an ion concentration $a_j = \gamma_j C_j$. Caution should be exercised when calculating junction potentials for the r-ED cell. Unlike electrodialysis stacks, where the effects of the junction potentials due to the electrode rinse compartment are ignored on account of large stack sizes, electrode rinse solutions can significantly affect the minimum operating potential in an r-ED cell. Taking note of the directionality of the electromotive forces generated at the permselective interfaces, potentials between the redox and diluate chamber, as well as the diluate chamber and concentrating chamber, will be net positive. In contrast, the potential between the redox and concentrate compartment will generally be net negative, barring very high NaCl concentrations in the concentrating chamber. For IEMs used in this study, the manufacturer reported the following permselectivity values: $t_+ = 0.96 - 0.99$ and $t_- = 0.94 - 0.97$ respectively. To simplify our analysis, it is assumed both AEM and CEMs are ideal, thus $t_+ = 1$ or $t_- = 1$; integrating the Eq. 19 results in:

$$E_J = -\frac{RT}{z_j F} \ln \frac{\gamma_j^\beta C_j^\beta}{\gamma_j^\alpha C_j^\alpha} \quad [20]$$

It is important to note from a practical standpoint that no single membrane transport number can serve as a universal descriptor of membrane permselective behavior. Geise et al. demonstrate that even 1:1 electrolytes such as NaCl and NH_4Cl exhibit different AEM permselective behavior, i.e. different transport numbers, which is attributed to differences in cation charge density.[38]

In the diluate and concentrating compartments, extensions of Debye-Huckel can provide accurate estimations of activity for NaCl solutions within the range $0.001\ \text{M} \leqslant C \leqslant 0.5\ \text{M}$, where concentration is in units of molarity:[14,21,22]

$$-\log\gamma = \frac{0.5065\sqrt{C}}{1 + 1.298\sqrt{C}} - 0.039C \quad [21]$$

Accurate calculation of the mean activity is more complicated for the outer compartments, as many ion species coexist within the phase, i.e., redox-active ions and supporting electrolytes. While activity models such as the Pitzer model or Specific Ion Interaction Theory (SIT) can be used for more complex solutions, both require *a priori* knowledge of parameters specific to a particular ionic species. To the best of our knowledge, these parameters have not been reported in the literature for the ferro/ferricyanide redox couple; thus, the mean activity of the outer two compartments is obtained manually fitting Eq. 19 to junction potential measurements, following the procedure detailed in *Junction Potential Measurements* section of this paper. Because the concentration of the outer two compartments is nearly constant for the duration of desalination experiments, it is assumed the fitted activity coefficient, $\gamma_{Redox} = 0.61$, is also constant.

Modeling—ohmic losses.—The general expression for the ohmic overpotentials within the r-ED cell is:

$$\eta_{ohmic} = \frac{I}{A} \sum_j l_j \rho_j \quad [22]$$

where l_j is the thickness of a particular medium, and ρ_j is the resistivity of the corresponding cell component. The woven nylon meshes are used as a spacer to generate turbulence in the channel as well as serve as a barrier preventing contact between the membranes; subsequently, the active area $A = \nu A_{geo}$ where ν is the fraction of open area of the nylon mesh, and A_{geo} is the geometric cell area ($7.00\ \text{cm} \times 3.65\ \text{cm}$). Boundary layer resistances of the concentrating and diluting compartments are also accounted for by approximating the boundary layer thickness, δ, as the ratio of

diffusivity of NaCl at infinite dilution and mass transfer coefficient.[39] Boundary layer concentrations are estimated as the average between the bulk and membrane surface concentrations.

$$\delta \approx \frac{D_{aq}}{k_m} \quad [23]$$

$$C_{BL} = \frac{C^{wall} + C^{bulk}}{2} \quad [24]$$

Note that the medium thickness l_j is equal to δ for boundary layers, $L - 2\delta$, the difference of membrane gap length and the boundary layers for the concentrating and diluting compartments, and L is the distance between the electrodes and membranes in the rinse compartments.

The resistivity of the concentrating and diluting solutions, as well as the boundary layers, can be calculated via the equivalent conductance of the solution:

$$\rho_{NaCl} = \frac{1}{C\Lambda} \quad [25]$$

where Λ is the equivalent conductance. The equivalent conductance of the concentrating or diluting NaCl solution can be estimated accurately up to a 100 mM concentration using the Falkenhagen equation, where the concentration has units of molarity.[40] The parameters Λ_0, B_1, B_2, and u can be found in (Table I).

$$\Lambda = \Lambda_0 - (B_1\Lambda_0 + B_2)\frac{\sqrt{C}}{1 + B_0 u\sqrt{C}} \quad [26]$$

The resistivities of each of the IEMs are calculated using the manufacturer-reported specific conductivities:

$$\rho_{Membrane} = \frac{1}{\kappa_{Membrane}} \quad [27]$$

where κ is the conductivity of the AEM or CEM. For this work, resistances resulting from the membrane are presumed to be constant, even though they are known to depend on solution concentrations interfacing on either side of the membrane.[41,42]

Lastly, the Nernst-Planck theory of an ideal electrolyte estimates the resistivity of outer channels containing multiple ionic species, where concentrations are held constant at the initial solution composition:

$$\rho_{Redox} = \frac{1}{F\sum_i |z_i|\ C_i u_i} \quad [28]$$

where the index indicates a particular ion species, and u_i is the ionic mobility of a particular species. Ionic mobilities are related to the diffusion coefficient of the ionic species through the Nernst-Einstein relation. Often ionic mobilities, diffusion coefficients, or both are tabulated throughout the literature.[43]

Modeling—electrode kinetics.—The activation overpotential contributions to the voltage loss in r-ED were accounted for using Butler-Volmer kinetics for a single-electron transfer with ferro/ferricyanide on graphitic carbon.

$$i = i_a + i_c = i_o\left[\exp\left(\frac{\alpha_a F}{RT}\eta_s\right) - \exp\left(-\frac{\alpha_c F}{RT}\eta_s\right)\right] \quad [29]$$

The subscripts a and c pertain to the anodic and cathodic reactions, i is the current density, i_o is the exchange current density, α is the charge transfer coefficient, which is assumed to be constant with potential, and η_s is the surface overpotential, also commonly referred to as the activation overpotential. To determine the kinetic parameters i_o, α_a, and α_c, the Tafel expressions are fit to rotating disc electrode (RDE) data obtained from Chen et al. when $|\eta_s| \gg 0$, i.e. the system is far from equilibrium.[12] The Tafel expressions for the anodic and cathodic currents are respectively;

$$i = i_o \exp\left(\frac{\alpha_a F}{RT}\eta_s\right) \quad \eta_s \gg 0 \quad [30]$$

$$i = -i_o \exp\left(-\frac{\alpha_c F}{RT}\eta_s\right) \quad \eta_s \ll 0 \quad [31]$$

Fit charge transfer coefficients were found to be $\alpha_a \approx \alpha_c = 0.5$. Since RDE experiments were performed at maximum concentrations of 10 mM ferrocyanide and 10 mM ferricyanide, respectively; the exchange current must be corrected for higher concentrations used in desalination experiments, using a reference concentration. Equation 32 calculates the concentration correction for the exchange current density. This equation's subscripts o and r represent the reduced and oxidized species. When using this equation, we assumed that $\lambda_1 = \lambda_2 = 0.5$ (for a single electron transfer), or by simultaneously fitting the λ_1 and λ_2 to a series of measured exchange current densities at varied concentration values.[44] Both methods provided the distribution range for the exchange current density values listed in (Table II).

$$i_o = i_{o,ref}\left(\frac{C_o}{C_{o,ref}}\right)^{\lambda_1}\left(\frac{C_r}{C_{r,ref}}\right)^{\lambda_2} \quad [32]$$

Calculation of desalination performance metrics.—The volumetric energy demand was determined using Eq. 33:

$$E_V = \frac{1}{V_D^T}\int_0^t IV(t)dt \quad [33]$$

where V_D^T is the diluate reservoir volume, and $V(t)$ is the voltage, which is a function of time. Note, the energy demand per salt removed can also be determined using Eq. 34. Here, C_0 is the initial concentration, and C_f is the final concentration.

$$E_{\mathrm{NaCl}} = \frac{1}{(C_0 - C_f)V_D^T}\int_0^t IV(t)dt \quad [34]$$

The average salt removal rate (ASRR) is used to quantify the removal rate of a given process and is calculated by;

$$ASRR = \left(\frac{C_0 - C_f}{t}\right)\frac{V_D^T}{A_{geo}} \quad [35]$$

Thermodynamic efficiency is simply the ratio of the thermodynamic volumetric energy demand (E_{Thermo}) and process volumetric energy demand.

Table I. Parameters for the Falkenhagen equation at 25 °C.[40]

Parameter	Value at 25 °C
Λ_0 (S-cm^2/mol)	126.45
B_0	0.3286
B_1	0.2289
B_2	60.32
u(Å)	4

Table II. Model parameters chosen for global sensitivity analysis and their ascribed bounds.

Parameter	Value	Bounds (%)	Reference
Spacer open area fraction: v	0.44	±10[a)]	This Work
Channel width: L (mm)	1	±20[b)]	This Work
Overall mass transfer coefficient: k_m (m/s)	7.4e-5[c)]	±10[c)]	34
Exchange current density: i_o (A/m^2)	74[c)]	±40[c)]	12
AEM conductivity: κ_{AEM} (mS/cm)	5.5	±20	This Work
CEM conductivity: κ_{CEM} (mS/cm)	4.5	±10	This Work
Membrane diffusion coefficient: D_m(m^2/s)	1.3e-11[e)]	±20[a)]	53
Electrode rinse mean activity coefficient (MAC): γ_R	0.61	±30[a)]	This Work

a) Conservative assumption on parameter error given variation in cell construction, error is equivalent to approximately a 1cm^2 variation in the active membrane area. b) Value estimated from experiment. c) Value estimated for this work's system based on methods or experiment of the relevant reference. d) Manufacturer product specification at 0.5 M NaCl through plane measurements. e) Assumed diffusion coefficient developed for Fumasep FAD/FKD membrane system is similar to that of this work.

$$\eta_{Thermo} = E_{Thermo}/E_v \quad [36]$$

and

$$E_{Thermo} = 2RT\left[\frac{C_0}{W_R}\ln\left(\frac{C_C}{C_0}\right) - C_D\ln\left(\frac{C_C}{C_D}\right)\right] \quad [37]$$

where, C_C is the final brine concentration and C_D is the final diluate concentration, and W_R is the water recovery defined as:

$$W_R = \frac{V_D^T}{V_C^T + V_D^T} \quad [38]$$

where V_C^T is the concentrate reservoir volume.

Propagation of error and global sensitivity analysis.—It is pertinent to perform a global sensitivity analysis to determine which parameters have the largest effect size in a modeling framework. The total Sobol index, S_T, was calculated for both reservoir concentrations and operating voltage at time steps throughout the desalination process. Total Sobol indices represent the total effect a particular model parameter has on outputs, including effects that interact with other parameters. Larger indices indicate a larger influence a particular parameter has on a given model output; at present, significant parameters are considered to have $S_T > 0.05$. To quantify uncertainties within the model, relevant input parameters were bounded to a range of possible values based on the magnitude of experimental error, calculated estimates, or conservative assumptions. Parameter space was sampled as a uniform distribution using a Saltelli sequence, where $N = 1024$. Model outputs (i.e., concentrations, voltages, and energy demands) were calculated using the generated input matrix. All examined parameters, their average value, and the assigned error estimate are found in (Table II). Given the non-normality of model outputs, bootstrapping was employed to calculate the relevant statistics of a given model output, such as means and standard deviations. Complementing analysis of the propagation of error, global sensitivity analyses (GSA) were performed by calculating the Sobol indices to determine which input parameters result in the most significant effect size on a particular model output.[45,46] All calculations were performed using Python version 3.11.4. GSAs were performed using the SAlib package, version 1.4.7.

Results and Discussion

Model validation.—To confirm the accuracy of each part of the model, we used resistance measurements and junction potentials as a benchmark against which to compare our theoretical calculations. The whole cell area specific resistance (i.e., the combination of all sources of ohmic resistances within the cell) was directly measured using EIS. Measurements were taken at two initial NaCl concentrations, 50 mM and 20 mM, corresponding to feed concentrations used for desalination experiments. As expected, a 50 mM chamber concentration has a considerably lower resistance compared to a 20 mM chamber concentration (Fig. 2A). Both the 50 mM and 20 mM conditions also exhibited considerable variation between replicate measurements. Variations in resistance are likely a result of variability in the membrane gap length due to inconsistencies in the cell stack pressure, leading to alterations in gasket compression. Under the assumption that the source of all error is deviations in gap length, as little as ≈0.2 mm gap length variability could account for the observed error. To account for these variations, the gap length model parameter was bounded with a range of ±20% the nylon spacer thickness. Overall, there is good agreement between the modeled calculations and experimental results, with slight underestimations and slight overestimations at 50 mM and 20 mM, respectively (Fig. 2A).

The AEM and CEM junction potentials were then experimentally measured in an H-cell set-up at varied compartment concentrations. In both cases, we observed the anticipated trends: a decrease in potential as the compartments attain similar ionic strengths. This observation aligns with the logarithmic expressions for permselective interfaces. For AEM junctions, the theoretical value only overestimates the experimental result by ⩽8 mV (Fig. 2B). This result also indicates that the extension of Debye-Huckel is a suitable activity model for the AEM junction. Measured CEM junctions were used to fit the activity coefficient of the outer electrode rinse solution, where the fitted activity coefficient for the outer electrolyte rinse solution (γ_{Redox}) was 0.61. A conservative error estimate of ±30% is imposed on the fitted activity coefficient. To our knowledge, activity model parameters for the ferro/ferricyanide redox couple do not exist in the literature. This leads to an unfortunate consequence of requiring activity measurements any time the concentration of the redox couple is significantly changed. However, if the relevant information does exist for a particular redox couple, more advanced activity models, such as specific ion interaction theory (SIT) or the Pitzer model, can be easily implemented. Even with the imposed parameter error, there is substantial agreement with experiment (Fig. 2C). It is also interesting to note that a negative potential will be generated at the concentrate-rinse junction because of high cation concentration in the outer channel, except for when desalinating highly concentrated brines. Ultimately, this produces a canceling effect with the juxtaposed diluate-rinse junction, where potentials resulting from either CEM junction produce electromotive forces with comparable magnitudes but opposite directions.

Batch-mode desalination experiments were carried out under three different operating conditions: Case 1) Equal volumes (50% water recovery) of 50 mM feeds with an applied current of 63 mA (geometric current density of 2.47 mA cm^{-2}); Case 2) volumes equal to a 71% water recovery, with a feed of 20 mM and an applied

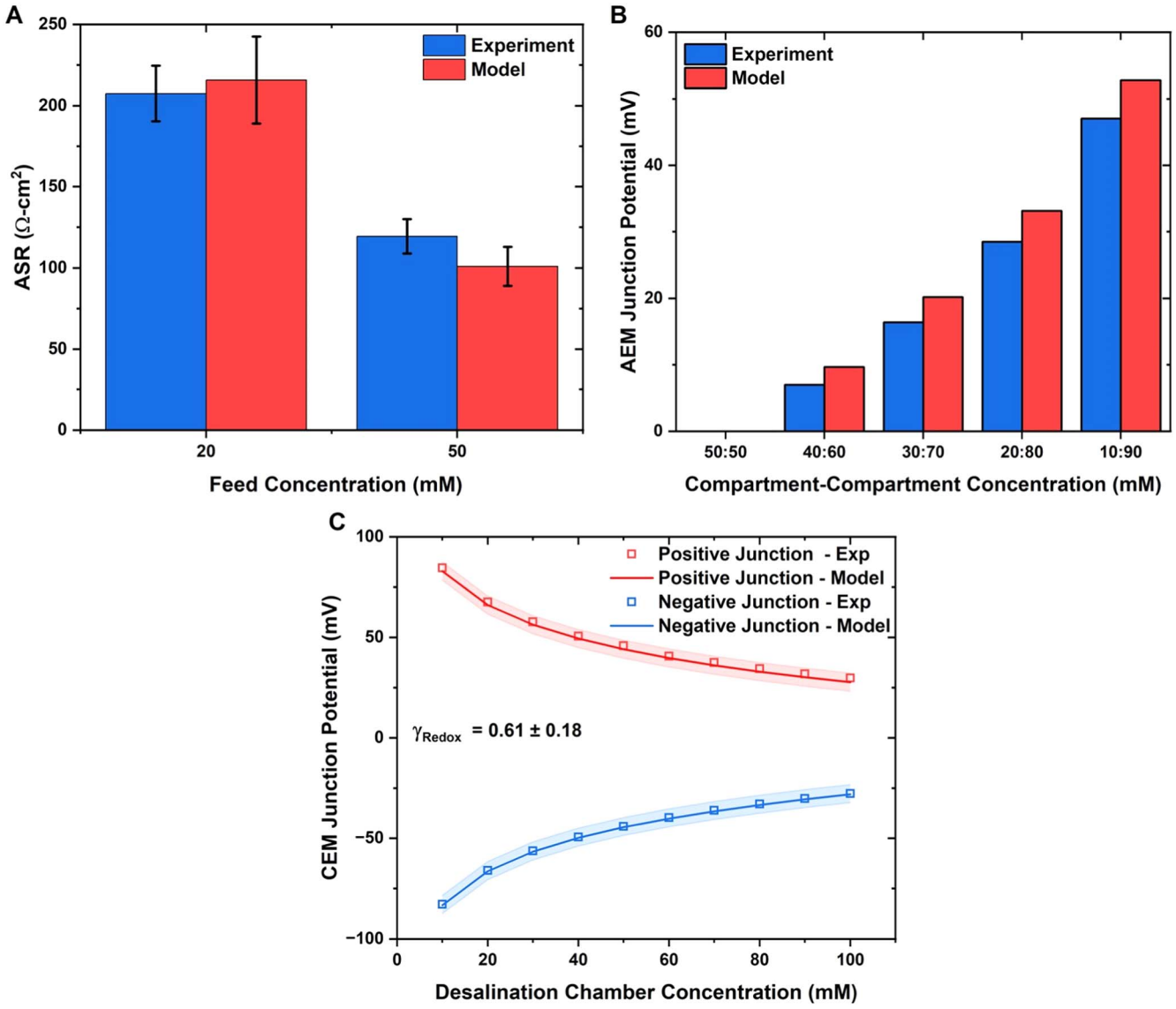

Figure 2. (A) A comparison between experimental and theoretical ASRs at 20 mM and 50 mM feed concentrations. (B) A comparison between experimental and theoretical AEM junction potentials assuming ideal membranes. (C) A comparison between experimental and theoretical CEM junction potentials between the redox channel and concentrate/diluate channels. Error bars and bands represent one standard deviation.

current of 63 mA (geometric current density of 2.47 mA cm^{-2}); Case 3) equal volumes (50% water recovery) of 20 mM feeds with an applied current of 126 mA (geometric current density of 4.93 mA cm^{-2}). For all three cases, reservoir concentration changes exhibit strongly linear behavior, which is expected considering electrolysis processes are described by Faraday's law, and water transport resulting from osmosis and electro-osmosis was observed to be 2%–5% by mass (Figs. 3A–3C). Case 2, which operates at a higher water recovery, also displays asymmetric concentration profiles, with the concentrate reservoir reaching much higher concentrations as expected from its much lower volume relative to the diluting reservoir. Case 3 could not reach potable drinking concentrations due to the imposed 1.6 V cell operating limit; thus, subsequent metrics are calculated at a final concentration of 12 mM. Experimental current efficiencies for cases 1–3 are 98% ± 2%, 97% ± 2%, and 92% ± 3%, respectively. Because little water transport was observed, the cell construction was sealed, and operating voltages were limited to 1.6 V to mitigate parasitic side reactions, it is inferred that current efficiencies less than unity arise from back diffusion of ions across the membranes.

All three cases display similar voltage profiles, with rapid voltage increases near the end of the desalination process as charge carriers become depleted from the diluting stream (Figs. 3D–3F). The experimental error in the voltage of case 3 is also significantly larger than for cases 1 and 2. This is attributed to deviations in the system's area specific resistance, as differences as small as 1 Ω can lead to change in observed potential that are proportional to the applied current. Furthermore, the magnitude of error tends to increase over the course of desalination. This is elucidated by considering that even relatively minor deviations in NaCl concentration between desalination runs lead to significant changes in observed voltage at low concentrations (Fig. S1). The resulting thermodynamic efficiencies calculated from the various desalination experiments range from 1.64% to 13.9%, which is comparable to other reports in the literature.[47]

Results from the developed model were compared to the experimental results from each of the three cases. Concentration profiles show good agreement in all three cases, with mean absolute error (MAE) values less than 2 mM (Table S1). Considering acceptable model error in conjunction with the model's assumption

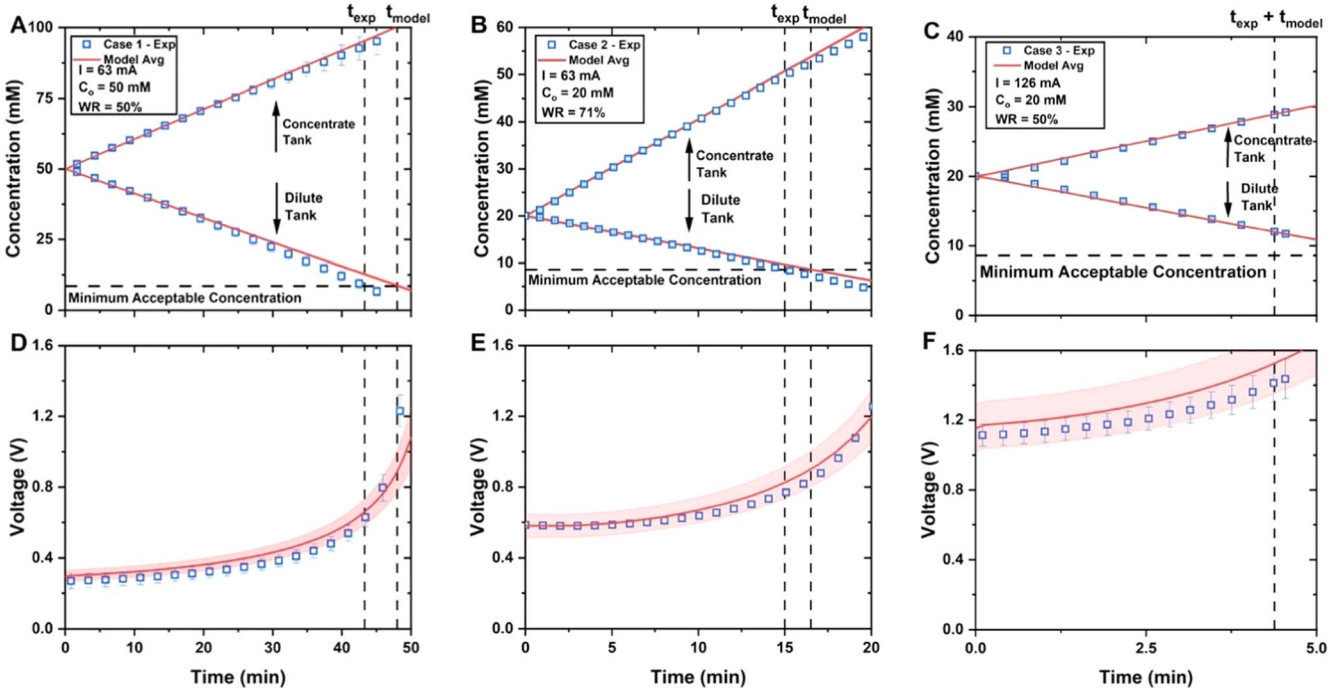

Figure 3. (A)–(F) Concentration and voltage profiles of various operating conditions compared to model predictions. Indicated times, t_{exp} and t_{model}, indicate the experimental and theoretical times required to reach a minimally acceptable drinking concentration, or 12 mM for 126 mA operation, as the cutoff voltage was reached before a complete desalination. Error bars, n = 3, 3, 6 for cases 1–3 respectively, and bands represent one standard deviation. If the error bar or band is not visualized, the error is comparable to the size of marker or line.

Table III. Experimental and theoretical desalination performance metrics of batch r-ED processes.

Operating conditions	Productivity (L-m^{-2}-h^{-1})	E$_v$(W-h-L^{-1})	ASRR (g-m^{-2}-min^{-1})	η_{Thermo}(%)
Case 1 BM: 63 mA | 50 mM Feed | 50% WR	21.7 ± 0.4	0.40 ± 0.050	0.88 ± 0.02	13.9 ± 1.6
Model–t_{exp}	N/A	0.45 ± 0.05	0.79 ± 0.01	N/A
Model–t_{model}	19.5 ± 0.3	0.55 ± 0.06	0.79 ± 0.01	10.1 ± 1.1
Case 2 BM: 63 mA| 20 mM Feed | 71% WR	78.4 ± 1.3	0.20 ± 0.01	0.87 ± 0.02	7.0 ± 0.2
Model–t_{exp}	N/A	0.20 ± 0.02	0.79 ± 0.01	N/A
Model–t_{model}	70.8 ± 1.2	0.23 ± 0.03	0.79 ± 0.01	5.9 ± 0.7
Case 3 BM: 126 mA | 20 mM Feed | 50% WR	213.9 ± 5.8	0.28 ± 0.02	1.66 ± 0.05	1.6 ± 0.1
Model	214.3 ± 1.8	0.30 ± 0.03	1.67 ± 0.01	1.5 ± 0.2
Case 4 SP: 63 mA | 50 mM | 36 ml min^{-1}	N/A	0.0091	1.20	N/A
Model	–	0.0087 ± 0.0010	0.89 ± 0.00	–
Case 5 SP: 252 mA | 50 mM | 36 ml min^{-1}	–	0.14	3.48	–
Model	–	0.14 ± 0.014	3.57 ± 0.00	–
Case 6 SP: 126 mA | 50 mM | 18 ml min^{-1}	–	0.072	1.39	–
Model	–	0.070 ± 0.075	1.79 ± 0.00	–
Case 7 SP: 50 mA | 50 mM | Q_{Dil} = 3.70 ml min^{-1} Q_{Con} = 3.50 ml min^{-1}	–	0.067	0.85	–
Model	–	0.059 ± 0.006	0.70 ± 0.00	–
Case 8 SP: 50 mA|50 mM|Q_{Dil} = 1.85 ml min^{-1} Q_{Con} = 1.70 ml min^{-1}	–	0.15	0.64	–
Model	–	0.14 ± 0.01	0.69 ± 0.00	–

BM indicates batch mode operation; SP indicates single pass operation. Batch mode model predictions are calculated for both the experimental time, t_{exp}, and theoretical time, t_{model}, i.e. the minimal acceptable drinking concentration is reached, or 12 mM in case 3, where there is no deviation in productivity between experiment and the model. Single pass operation metrics are calculated as an average of the steady state. Errors signify one standard deviation.

of $\varphi \approx 1$, it is reasonable to conclude that ion back diffusion is responsible for experimental current efficiencies less than unity, as diffusion is the only mechanism that could result in lowered current efficiencies accounted for in the model. There was a tendency for the model to overpredict concentrations, leading to a lag in predicted desalination time that can reach several minutes. Subsequently, this tendency leads to lower predicted production rates and ASRRs, on the order of ∼10%, compared to the experimental values (Table III). This also suggests that the experimental system's back diffusion is not as severe. Predicted voltage profiles also agree with experimental results, with MAEs no more than 74.9 mV (Table S1). Considering energy expenditures for desalination depend on time, delays produce overestimations. Ultimately, this only leads to considerable overestimations at the longest desalination times; nonetheless, agreement

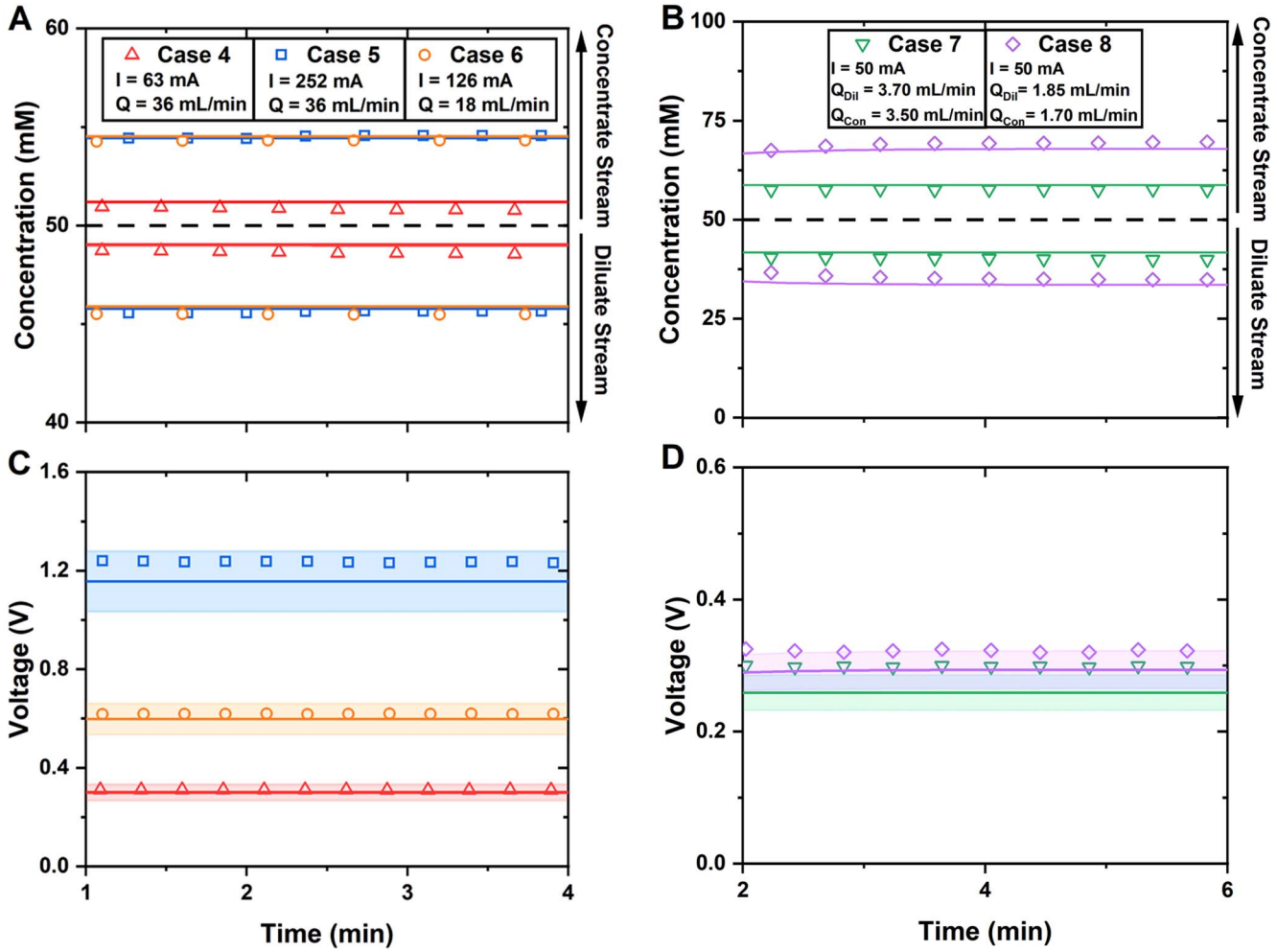

Figure 4. (A), (B) Steady-state concentration profiles for single-pass desalination operating conditions Cases 4–8. Values above the feed line correspond to the concentrating stream, whereas values below correspond to the diluting stream. (C), (D) Steady-state voltage profiles operating conditions Cases 4–8. Solid lines indicate model averages, error bands, and bars represent one standard deviation of the model output.

between experimental and model energy metrics is restored if metrics are compared over the same operating duration.

Single-pass r-ED desalination experiments for Cases 4–8 were conducted under varied applied currents and flow rates (Table III). All cases display expected steady-state behavior, with concentration changes in the concentrate and diluate being approximately equal in magnitude (Figs. 4A, 4B). Comparing cases 4 and 5, it is again demonstrated that the system strongly concords with Faraday's law, i.e., increasing current increases salt removal. Cases 5 and 6 also illustrate this behavior as the degree of salt removal between the two conditions is indistinguishable when the ratio between applied current and residence time remains unchanged. This fact is essential for design considerations, as the operating voltage, and closely related energy demands, can be significantly reduced, albeit at the expense of production rates (Figs. 4C, 4D). Furthermore, it is possible to achieve very high levels of salt removal simply by lowering the system flow rate, as demonstrated in cases 7 and 8.

The model was also applied to each case of single-pass operation by simply removing the concentrate and diluting reservoir mass balance equations. Concentration profiles strongly agree with MAEs less than 1 mM across all cases (Table S2). It is also worth noting that the model is sensitive to even slight deviations in flow rates, particularly in Cases 7 and 8 at low flow conditions. The model reasonably captures voltage profiles for each of the five conditions. There is a tendency to underpredict potentials at high current conditions, such as in Case 5, and low flow-rate conditions, such as in Cases 7 and 8; even so, the MAE for each case is acceptable, with values of 75.5 mV, 39.6 mV, and 29.4 mV respectively (Table S2). Modeled salt removal and energy metrics are also in reasonable agreement with experiment (Table III).

Ion-exchange resin wafer implementation.—While implementation of ion-exchange resin wafers for EDI has historically been considered to be operationally difficult on account of leaks, increased flow resistance leading to pressure drops, and subsequently increased pumping energy demands, an unoptimized ion exchange resin wafer was implemented in the cell's diluate channel to reduce the ohmic overpotentials within the system.[23] This demonstration is intended to show that combating ohmic losses can significantly reduce energy demands of the r-ED platform, as observed in similar systems.[23,25,26,48,49] The cell was operated under the same experimental conditions as in Case 3. Average salt removal rates between the RW and no RW case are indistinguishable. The resin wafer implementation did, however, reduce the volumetric energy demand by ∼18%. Comparing voltage profiles at the same operating conditions with and without the RW, the voltage of the system with the RW is significantly lower and remains in an operating window where electrode corrosion is of little concern.

Ion exchange membranes can comprise a significant portion, if not most, of the total capital cost of a desalination unit.[50] Given that current density is directly related to the ion flux through Faraday's law, increasing current density by RW implementation directly reduces the capital cost of the platform by enabling smaller cell area, with subsequently smaller membranes, and may enable small-

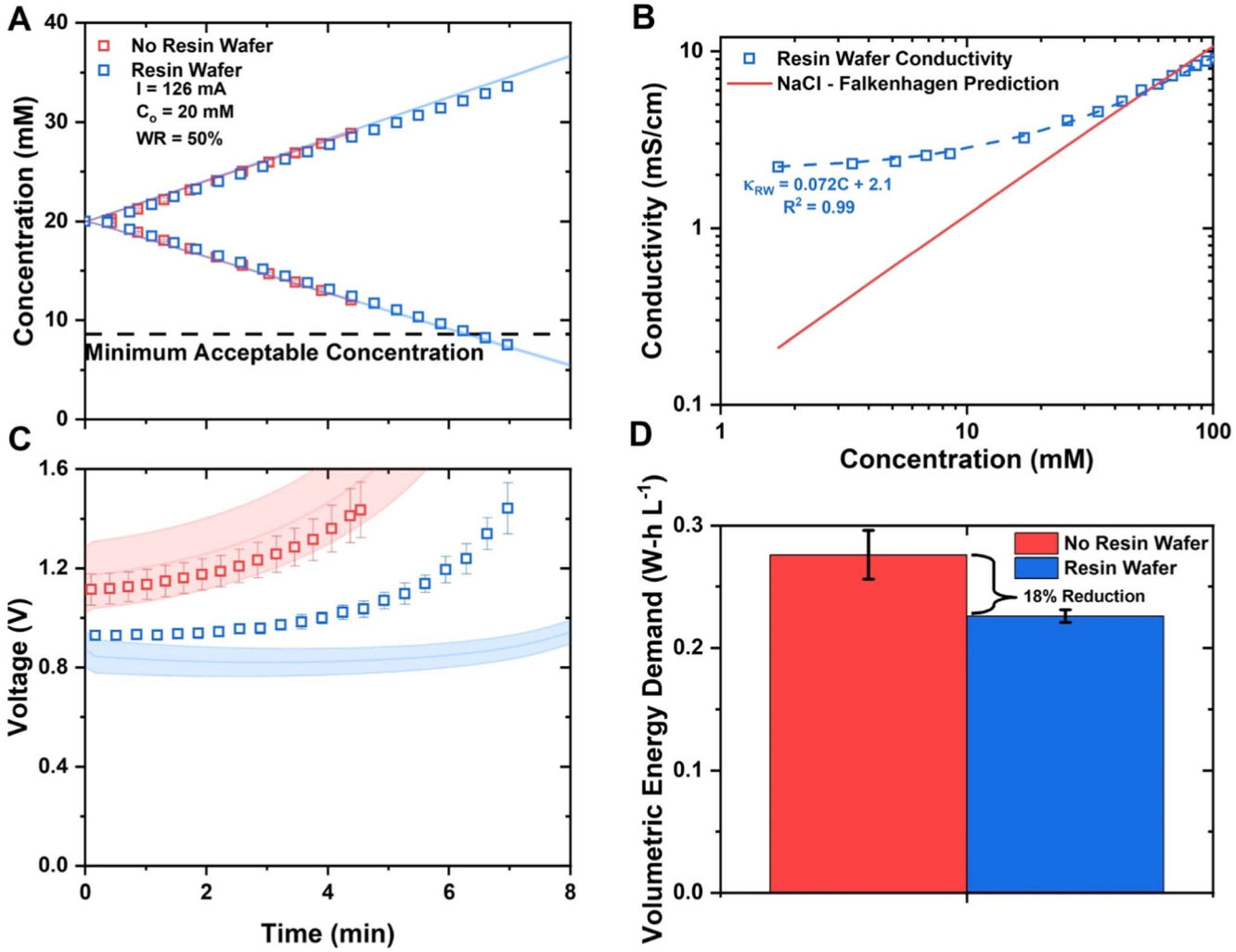

Figure 5. (A) Concentration profile comparing no resin wafer and resin wafer implementation. (B) Measured through-plane conductivity of the mixed resin wafer compared to the theoretical conductivity of NaCl solution predicted by the Falkenhagen equation. (C) The concentration profile's associated voltage profile. Solid lines represent model predictions, error bars and bands represent one standard deviation. (D) Energy metric comparison between no resin wafer and resin wafer implementation at a final concentration of 12 mM.

scale devices with practically relevant productivities for applications where ergonomic handling of the device is necessary; for instance, distributed freshwater production in remote locations. However, operation at larger current densities increase the cell's operating costs in terms of energy demand, thus cost minimization as a function of cell size and operating current for a particular production rate is open to case-by-case economic analysis. In our r-ED system, implementation of the RW clearly demonstrates that potable water can now be produced at current densities previously limited by practical cell operating voltages (Fig. 5A). At the same degree of salt removal, 20 mM to 12 mM, the resin wafer also reduced energy demands by ∼18% (Fig. 5D). Furthermore, by tuning resin wafer chemistry through ionomer binders in lieu of nonconductive polyethylene, ohmic losses may be curtailed further, leading to even higher current density operation and smaller units.[23]

The model was adapted in attempt to capture the behavior with RW implementation, using empirical relations and geometric estimates of the wafer. Water displacement measurements determined the free volume of the swollen wafer to be approximately 2.1 ml. The conductivity expression of the diluate chamber is also replaced by an empirical relation fit to through-plane conductivity measurements of the RW at varying NaCl concentration (Fig. 5B); hence, the open area fraction for the diluate compartment becomes unity. Predicted concentration profiles agree with the experimental results, further indicating that Faraday's Law and back diffusion adequately describe desalination behavior. (Fig. 5A). The modeled voltage profile does not capture system behavior. Predicted voltages were substantially lower than the experimental voltage and do not display a rapid voltage increase at low salt concentrations (Fig. 5C). The empirical resin wafer conductivity expression is derived from bulk measurements, which would capture the effects of the nonconductive binder and interstitial volumes between resin particles. These facts, in conjunction, indicate that a simple through-plane conductivity cell set-up grossly overestimates the conductivity measurements. The most likely reason for these overestimations is the presence of shunt currents during ex situ conductivity measurements. Shunt currents may be exacerbated by wafer defects, which can result from uneven distributions of porogen and by edge effects between the planar electrodes.

Sensitivity analysis.—Sensitivity analyses were performed for each of the three batch cases to determine which input parameters have the most significant effects on model outputs. Regarding reservoir concentrations, the total Sobol index, S_T, indicates the most sensitive parameter is the diffusion coefficient of NaCl through the membranes, which determines the extent of back diffusion across the membranes. To a lesser degree, the open area fraction, vF, also has a small role in model sensitivity, as it determines the effective

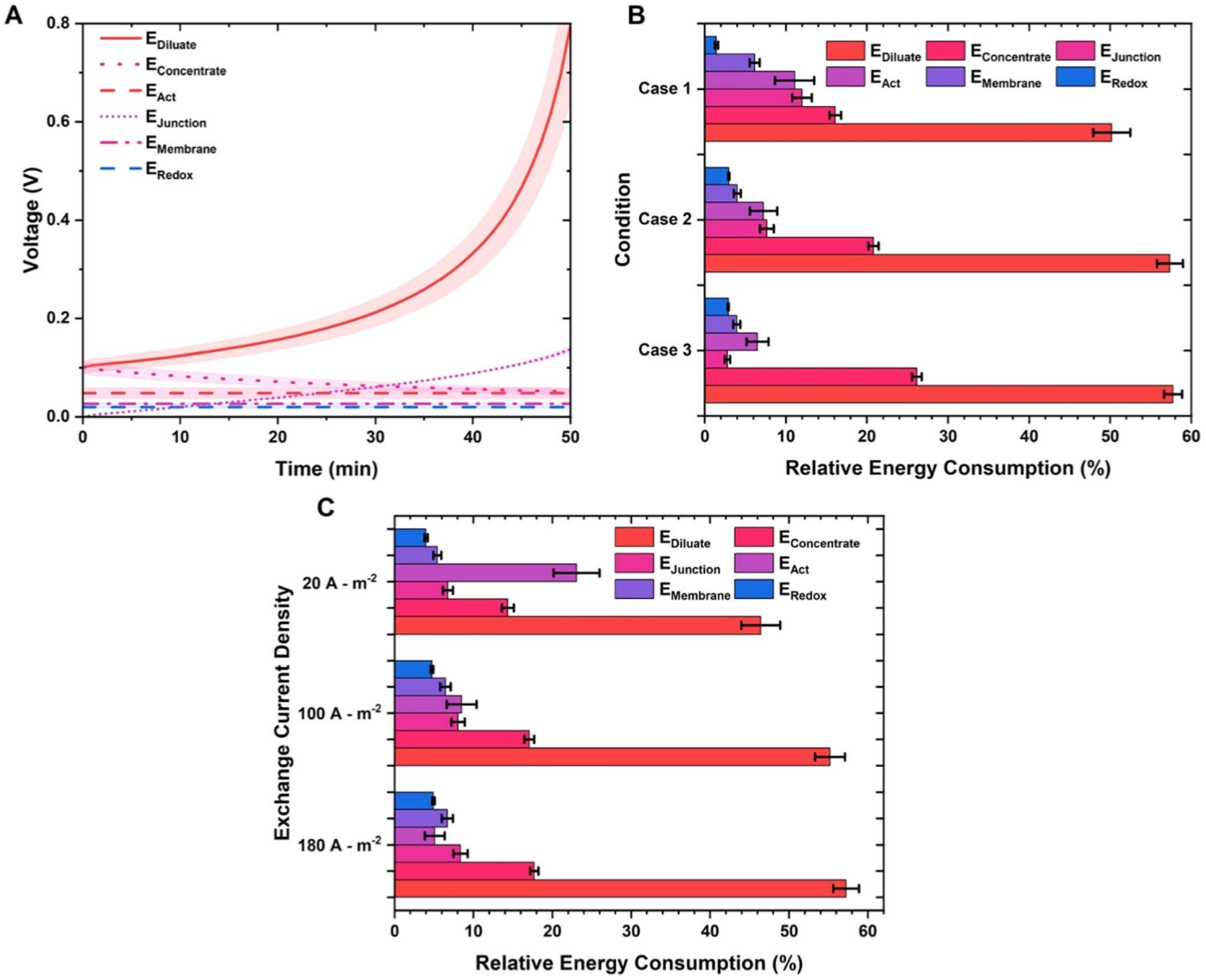

Figure 6. (A) Voltage breakdown for batch-mode case 1, 63 mA at 50% WR. (B) Relative energy consumptions for each voltage contribution for batch-mode cases 1–3. Error bands and error bars represent one standard deviation. (C) Relative energy consumptions for three hypothetical redox couples with varying kinetic properties.

membrane area where back diffusion occurs. All other parameters can be considered to produce insignificant effects on tank concentration throughout desalination. During most of the desalination process, the variance in cell voltage is dominated by the membrane gap length and, to a lesser extent, the open area fraction. However, at the longest desalination times, the membrane diffusion coefficient can have a significant contribution (Figs. S2–S3). At low salt concentrations slight deviations in concentration will lead to large swings in solution conductivity, as discussed earlier. There are no significant second-order parameter-parameter interactions for all model parameters and outputs to report.

Model comparison to existing literature.—There are several improvements afforded by this work over previous modeling r-ED efforts found in the literature.[14] While maintaining an acceptable degree of concordance between the model and a variety of experimental operating conditions, the model has reduced the number of adjustable fitting parameters from three to zero when compared to the model by Kim and coworkers.[14] Zero fitting parameters give greater confidence for rapid examination of case studies across a range of operating parameters. This is because each defined input is a material property or user-defined operating condition. In this work, mass balances have additional terms to account for diffusion between each channel, eliminating the need for fitted time parameters. Mass transfer effects due to channel spacers are also captured by employing relations developed previously in literature. Moreover, voltage calculations include coarse approximations, boundary layer resistances, electrode reactions—which are typically ignored—and they individually account for junction potentials present at each membrane. Furthermore, the implementation of the quasi-Monte Carlo algorithm facilitates a rigorous examination of error propagation and global sensitivity analyses, which have been lacking in r-ED models.

Voltage breakdown and electrode kinetics.—Given the model demonstrates an acceptable degree of prediction capability, the voltage contributions of cell components can be reliably calculated (Fig. 6A). Strikingly, all voltage contributions are minuscule compared to the diluate compartment's ohmic overpotential contribution, which ranges from 50.2%–57.8%. The next highest potential contribution is the concentrate stream**,** which only accounts for 16.1%–26.2% of energy requirement. Electrode reactions only consume 6.5%–11.1% of the total energy, which is marginal compared to the total energy requirement (Fig. 6B). Given the relatively low energy consumption contributions of the redox reactions, there is little motivation to find alternative redox

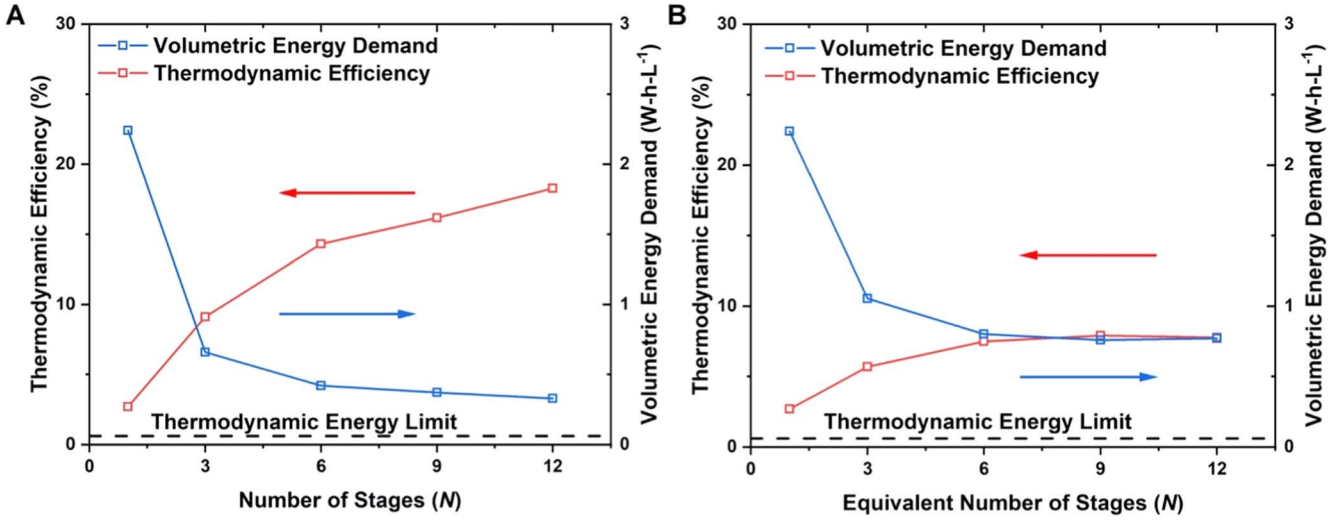

Figure 7. (A) Thermodynamic efficiency and volumetric energy demands for a multistage process. Theoretical current densities required to reach 8.6 mM final concentration are found in Table S3 (B) Thermodynamic efficiency and volumetric energy demands for a single-stage process with a cell area equivalent to *N* number of stages. Theoretical current densities required to reach 8.6 mM final concentration are found in Table S4. Points indicate calculated values using the average model input parameters' values. Feed conditions were 50 mM with 50% water recovery, with 2 ml min^{-1} flowrates.

chemistries for the electrodes that would lower the activation overpotentials. Consider three redox couples that display exchange current densities of 20 A m^{-2}, 100 A m^{-2}, and 180 A m^{-2}, respectively. Operating an r-ED batch cell with the same dimensions as those in this study, a desalination from 50 mM to 8.6 mM, at an applied current of 100 mA, would account for 23.1%, 8.5%, and 5.1% of the total energy expenditures (Fig. 6C). Compared to the relative energy consumption of the experimental batch operations, there is minimal reduction in process energy requirements to be gained by considerable improvements in electrode kinetics; even if a worst-case scenario was realized, electrode kinetics still do not comprise more than a quarter of the total energy demands. Of course, operating extremely large current densities using couples with even otherwise moderately facile kinetics can spur high overpotentials; practically, this is not possible in an r-ED desalination device since carbon electrode corrosion will limit the cell's practical operating potential. For these reasons, when choosing an appropriate redox chemistry, the criteria of low human and environmental toxicity and system stability should be paramount. Compounds such as viologens should be avoided, especially when producing water for human consumption.

Process design considerations.—With reasonable agreement across a variety of operating conditions, optimal cell configurations can be explored. Consider two styles of cell configurations: a multistage process consisting of cells of equal area with current distributed equally among them to reach 8.6 mM effluent and a single-stage process with a cell of increasing area equivalent to that of the total area between the cells comprising the multistage process. For this analysis, model parameters are set to the average value of each parameter, and diffusion from the redox compartments is ignored. Unsurprisingly, the multistage process achieves energy demands approaching the thermodynamic limit with increasing stages as a growing number of stages approaches that of a thermodynamically reversible process (Fig. 7A). This result is in agreement with analyses considering the thermodynamics of an electrochemical separation process; with increasing an increasing number of stages, the operating potential approaches that of the Donnan/equilibrium potential of a particular stage, i.e. overpotentials are limited.[51,52] Increasing the cell area within a single-stage process may also increase thermodynamic efficiency and reduce energy consumption as the operating current density is reduced; however, to a much smaller extent compared to the multistage process (Fig. 7B). A limitation of this analysis is that the model does not account for concentration gradients occurring along the length of the cell channel. Therefore, it is unclear how strongly plug flow behavior is exhibited as the cell is increasingly scaled in size, so it may be possible that a large cell area single-stage process will begin to behave similarly to a multistage process via plug flow behavior, depending on internal hydrodynamics. A more comprehensive analysis of internal flow behavior is required to elucidate the extent of salinity gradients that develop across the cell and guide optimal process designs.

Conclusions

A 0-fitting parameter r-ED model was developed, and it accurately captures the cell's voltage and effluent concentration profiles allowing for an intelligent approach when targeting various sources of overpotentials within the cell. It is important to note that while basic r-ED models exist in literature, they use too many adjustable parameters; hence, model accuracy across systems tends to suffer. By adopting an r-ED model zero fitting parameters—validated under different feed concentrations, current density values, and recirculation/single-pass modes—it is now possible to perform accurate techno-economic analysis of r-ED cells and provide insights into process design considerations. Voltage breakdowns provided by the model indicate that ohmic overpotentials resulting from the depletion of ions in the diluate stream are the most considerable overpotential contributions in the cell. This large overpotential can be ameliorated by employing porous ionic conductors, such as ion-exchange resin wafers, into the diluate chamber. We show a reduction of ∼18% in volumetric energy demand when using r-ED with an ion-exchange resin wafer in the diluate chamber and operating at a high current density-low salinity regime. Furthermore, we envision the model to be useful for gauging the performance of r-ED compared to other desalination platforms such as RO and traditional ED. These results culminate in several general considerations for researchers and device designers for electrochemical brackish water desalination using r-ED: (1) Efforts in identifying or improving electrode kinetics will afford relatively minor improvements in energy demands; therefore, inexpensive, nontoxic, and low IEM permeable compounds should be preferential. (2) Most cell energy expenditure results from ohmic resistances developed in the diluate chamber; to improve energy efficiency, research efforts should focus on reducing these ohmic losses, such as demonstrated here with ion-

exchange resin wafers. (3) Process design tradeoffs, such as increased energy expenditure for decreased cell size, and cells in series compared larger to single-cell units, require careful techno-economic analysis and lifecycle assessments.

Acknowledgments

This work was supported by the Office of Naval Research (ONR) through grant number N00014-22-1-2564. Any opinions, conclusions, or recommendations presented in this work do not necessarily reflect the views of the Office of Naval Research. We also acknowledge Teresea Pond for assistance in cell fabrication.

Code Availability

The underlying code for this study is not publicly available but may be made available on reasonable request to the corresponding authors.

Competing Interests

All authors declare no financial or non-financial competing interests.

Additional Information

Supplementary information is available for this paper.

ORCID

Timothy C. Hudak https://orcid.org/0009-0002-1889-8552
Christopher A. Gorski https://orcid.org/0000-0002-5363-2904
Christopher G. Arges https://orcid.org/0000-0003-1703-8323

References

1. Summary Progress Update: SDG 6 — water and sanitation for all, United Nations - Water (2021).
2. M. M. Mekonnen and A. Y. Hoekstra, "Four billion people facing severe water scarcity." *Sci. Adv.*, **2**, e1500323 (2016).
3. I. Kramer, Y. Tsairi, M. B. Roth, A. Tal, and Y. Mau, "Effects of population growth on Israel's demand for desalinated water." *Npj Clean Water*, **5**, 1 (2022).
4. J. S. Stanton et al., *Brackish Groundwater in the United States*, U.S. Geological Survey (2017).
5. H. Quon and S. Jiang, "Decision making for implementing non-traditional water sources: a review of challenges and potential solutions." *Npj Clean Water*, **6**, 1 (2023).
6. A. Boretti and L. Rosa, "Reassessing the projections of the world water development report." *Npj Clean Water*, **2**, 1 (2019).
7. D. Curto, V. Franzitta, and A. Guercio, "A review of the water desalination technologies." *Appl. Sci.*, **11**, 670 (2021).
8. M. A. Alkhadra et al., "Electrochemical methods for water purification, ion separations, and energy conversion." *Chem. Rev.*, **122**, 13547 (2022).
9. V. Pothanamkandathil and C. A. Gorski, "Comparing energy demands and longevities of membrane-based capacitive deionization architectures." *Environ. Sci. Water Res. Technol.*, **8**, 1489 (2022).
10. S. K. Patel, M. Qin, W. S. Walker, and M. Elimelech, "Energy efficiency of electro-driven brackish water desalination: electrodialysis significantly outperforms membrane capacitive deionization." *Environ. Sci. Technol.*, **54**, 3663 (2020).
11. R. Xie, D. Yue, Z. Peng, and X. Wei, "Achieving energy-saving, continuous redox flow desalination with iron chelate redoxmers." *Energy Mater. Adv.*, **4**, 0009 (2023).
12. F. Chen, J. Wang, C. Feng, J. Ma, and T. David Waite, "Low energy consumption and mechanism study of redox flow desalination." *Chem. Eng. J.*, **401**, 126111 (2020).
13. F. Chen, J. Wang, Q. Ru, S. H. Aung, T. Z. Oo, and B. Chu, "Continuous electrochemical desalination via a viologen redox flow reaction." *J. Electrochem. Soc.*, **167**, 083503 (2020).
14. G. Mohandass, S. Krishnan, and T. Kim, "Experimental analysis and modeling of closed-loop redox flow desalination." *J. Electrochem. Soc.*, **169**, 063521 (2022).
15. E. S. Beh, M. A. Benedict, D. Desai, and J. B. Rivest, "A redox-shuttled electrochemical method for energy-efficient separation of salt from water." *ACS Sustain. Chem. Eng.*, **7**, 13411 (2019).
16. Q. Zhang, S. H. Aung, T. Z. Oo, and F. Chen, "Continuous electrochemical deionization by utilizing the catalytic redox effect of environmentally friendly riboflavin-5'-phosphate sodium." *Mater. Today Commun.*, **23**, 100921 (2020).
17. N. Kim, J. Elbert, C. Kim, and X. Su, "Redox-copolymers for nanofiltration-enabled electrodialysis." *ACS Energy Lett.*, **8**, 2097 (2023).
18. N. Kim, J. Lee, and X. Su, "Precision tuning of highly selective polyelectrolyte membranes for redox-mediated electrochemical separation of organic acids." *Adv. Funct. Mater.*, **33**, 2211645 (2023).
19. D. Lu, C. Xu, Y. Wang, and W. Cai, "Continuous desalination via redox flow desalination using sodium 4-sulfonatooxy-2,2,6,6-tetramethyl-piperidine-1-Oxyl (NaSO4-TEMPO)." *Chem. Eng. J.*, **431**, 133917 (2022).
20. C.-Y. Cheng, T.-H. Chen, K.-Y. Chen, J. Ma, and C.-H. Hou, "Redox-flow battery with four-channel architecture for continuous and efficient desalination over a wide salinity working range." *Desalination*, **534**, 115783 (2022).
21. N. C. Wright, S. R. Shah, S. E. Amrose, and A. G. Winter, "A robust model of brackish water electrodialysis desalination with experimental comparison at different size scales." *Desalination*, **443**, 27 (2018).
22. J. M. Ortiz, J. A. Sotoca, E. Expósito, F. Gallud, V. García-García, V. Montiel, and A. Aldaz, "Brackish water desalination by electrodialysis: batch recirculation operation modeling." *J. Membr. Sci.*, **252**, 65 (2005).
23. V. M. Palakkal, L. Valentino, Q. Lei, S. Kole, Y. J. Lin, and C. G. Arges, "Advancing electrodeionization with conductive ionomer binders that immobilize ion-exchange resin particles into porous wafer substrates." *Npj Clean Water*, **3**, 1 (2020).
24. V. M. Palakkal, M. L. Jordan, D. Bhattacharya, Y. J. Lin, and C. G. Arges, "Addressing spacer channel resistances in MCDI using porous and pliable ionic conductors." *J. Electrochem. Soc.*, **168**, 033503 (2021).
25. S.-Y. Pan, S. W. Snyder, H.-W. Ma, Y. J. Lin, and P.-C. Chiang, "Development of a resin wafer electrodeionization process for impaired water desalination with high energy efficiency and productivity." *ACS Sustain. Chem. Eng.*, **5**, 2942 (2017).
26. S.-Y. Pan, S. W. Snyder, H.-W. Ma, Y. J. Lin, and P.-C. Chiang, "Energy-efficient resin wafer electrodeionization for impaired water reclamation." *J. Clean. Prod.*, **174**, 1464 (2018).
27. X.-Y. Zheng, S.-Y. Pan, P.-C. Tseng, H.-L. Zheng, and P.-C. Chiang, "Optimization of resin wafer electrodeionization for brackish water desalination." *Sep. Purif. Technol.*, **194**, 346 (2018).
28. A. Fasuyi and A. M. Lopez, "Influence of poly(ionic) liquid incorporation within resin wafer electrodeionization for reduced energy consumption in brackish water desalination." *Chem. Eng. J.*, **454**, 140209 (2023).
29. M. Tedesco, H. V. M. Hamelers, and P. M. Biesheuvel, "Nernst-planck transport theory for (reverse) electrodialysis: II. effect of water transport through ion-exchange membranes." *J. Membr. Sci.*, **531**, 172 (2017).
30. L. Han, S. Galier, and H. Roux-de Balmann, "Ion hydration number and electro-osmosis during electrodialysis of mixed salt solution." *Desalination*, **373**, 38 (2015).
31. T. Mohammadi, S. C. Chieng, and M. Skyllas Kazacos, "Water transport study across commercial ion exchange membranes in the vanadium redox flow battery." *J. Membr. Sci.*, **133**, 151 (1997).
32. D. K. Kim, S. J. Yoon, and S. Kim, "Transport phenomena associated with capacity loss of all-vanadium redox flow battery." *Int. J. Heat Mass Transf.*, **148**, 119040 (2020).
33. A. J. Bard, L. R. Faulkner, and H. S. White, *Electrochemical Methods: Fundamentals and Applications* (Wiley, New York) (2022).
34. A. R. Da Costa, A. G. Fane, and D. E. Wiley, "Spacer characterization and pressure drop modelling in spacer-filled channels for ultrafiltration." *J. Membr. Sci.*, **87**, 79 (1994).
35. S. Pawlowski, J. G. Crespo, and S. Velizarov, "Pressure drop in reverse electrodialysis: experimental and modeling studies for stacks with variable number of cell pairs." *J. Membr. Sci.*, **462**, 96 (2014).
36. D. A. Vermaas, E. Guler, M. Saakes, and K. Nijmeijer, "Theoretical power density from salinity gradients using reverse electrodialysis." *Energy Procedia*, **20**, 170 (2012).
37. G. Schock and A. Miquel, "Mass transfer and pressure loss in spiral wound modules." *Desalination*, **64**, 339 (1987).
38. G. M. Geise, H. J. Cassady, D. R. Paul, B. E. Logan, and M. A. Hickner, "Specific ion effects on membrane potential and the permselectivity of ion exchange membranes." *Phys. Chem. Chem. Phys.*, **16**, 21673 (2014).
39. V. Geraldes and M. D. Afonso, "Limiting current density in the electrodialysis of multi-ionic solutions." *J. Membr. Sci.*, **360**, 499 (2010).
40. G. Kortum, *Treatise on Electrochemistry* (Elsevier Science Ltd, Amsterdam) (1965), Revised edition.
41. A. H. Galama, N. A. Hoog, and D. R. Yntema, "Method for determining ion exchange membrane resistance for electrodialysis systems." *Desalination*, **380**, 1 (2016).
42. P. Długołęcki, P. Ogonowski, S. J. Metz, M. Saakes, K. Nijmeijer, and M. Wessling, "On the resistances of membrane, diffusion boundary layer and double layer in ion exchange membrane transport." *J. Membr. Sci.*, **349**, 369 (2010).
43. J. Newman and K. E. Thomas-Alyea, *Electrochemical Systems* (Wiley-Interscience, Hoboken, N.J) 3rd ed. (2004).
44. T. F. Fuller and J. N. Harb, *Electrochemical Engineering* (Wiley, New York) (2018).
45. M. Renardy, L. R. Joslyn, J. A. Millar, and D. E. Kirschner, "To sobol or not to sobol? the effects of sampling schemes in systems biology applications." *Math. Biosci.*, **337**, 108593 (2021).
46. X.-Y. Zhang, M. Trame, L. Lesko, and S. Schmidt, "Sobol sensitivity analysis: a tool to guide the development and evaluation of systems pharmacology models." *CPT Pharmacomet. Syst. Pharmacol.*, **4**, 69 (2015).
47. G. Mohandass, W. Chen, S. Krishnan, and T. Kim, "Asymmetric and symmetric redox flow batteries for energy-efficient, high-recovery water desalination." *Environ. Sci. Technol.*, **56**, 4477 (2022).
48. M. L. Jordan, G. Kokoszka, H. K. Gallage Dona, D. I. Senadheera, R. Kumar, Y. J. Lin, and C. G. Arges, "Integrated ion-exchange membrane resin wafer assemblies for aromatic organic acid separations using electrodeionization." *ACS Sustain. Chem. Eng.*, **11**, 945 (2023).

49. P.-C. Tseng, Z.-Z. Lin, T.-L. Chen, Y. Lin, and P.-C. Chiang, "Performance evaluation of resin wafer electrodeionization for cooling tower blowdown water reclamation." *Sustain. Environ. Res.*, **32**, 36 (2022).
50. H. Strathmann, A. Grabowski, and G. Eigenberger, "Ion-exchange membranes in the chemical process industry." *Ind. Eng. Chem. Res.*, **52**, 10364 (2013).
51. S. Lin, "Energy efficiency of desalination: fundamental insights from intuitive interpretation." *Environ. Sci. Technol.*, **54**, 76 (2020).
52. L. Wang, C. Violet, R. M. DuChanois, and M. Elimelech, "Derivation of the theoretical minimum energy of separation of desalination processes." *J. Chem. Educ.*, **97**, 4361 (2020).
53. J. Veerman, R. M. de Jong, M. Saakes, S. J. Metz, and G. J. Harmsen, "Reverse electrodialysis: comparison of six commercial membrane pairs on the thermodynamic efficiency and power density." *J. Membr. Sci.*, **343**, 7 (2009).